# Physics-Informed Neural Network for Modelling the Thermochemical Curing Process of Composite-Tool Systems During Manufacture

Sina Amini Niaki<sup>a,c</sup>, Ehsan Haghighat<sup>c</sup>, Xinglong Li<sup>b</sup>, Trevor Campbell<sup>b,a</sup>, Reza Vaziri<sup>c</sup>

<sup>a</sup>Data Science Institute (DSI), The University of British Columbia

<sup>b</sup>Department of Statistics, The University of British Columbia

<sup>c</sup>Composites Research Network (CRN), Departments of Civil Engineering and Materials Engineering, The

University of British Columbia

#### Abstract

We present a Physics-Informed Neural Network (PINN) to simulate the thermochemical evolution of a composite material on a tool undergoing cure in an autoclave. In particular, we solve the governing coupled system of differential equations—including conductive heat transfer and resin cure kinetics—by optimizing the parameters of a deep neural network using a physics-based loss function. To account for the vastly different behaviour of thermal conduction and resin cure, we design a PINN consisting of two disconnected subnetworks, and develop a sequential training algorithm that mitigates instability present in traditional training methods. Further, we incorporate explicit discontinuities into the DNN at the composite-tool interface and enforce known physical behaviour directly in the loss function to improve the solution near the interface. Finally, we train the PINN with a technique that automatically adapts the weights on the loss terms corresponding to PDE, boundary, interface, and initial conditions. The performance of the proposed PINN is demonstrated in multiple scenarios with different material thicknesses and thermal boundary conditions.

Keywords: Physics-Informed Neural Networks, Deep Learning, Composites Processing, Exothermic Heat Transfer, Cure Kinetics, Resin Reaction

# 1. Introduction

The manufacture of polymeric composite materials involves forming prepreg, e.g. carbon fibres in a resin system, on a tool followed by subjecting the composite-tool system to a controlled cycle of temperature inside an autoclave [1]. The elevated temperature within the autoclave cures the polymeric resin resulting in a final composite product. The physics of this thermochemical process is well-established and expressed by a set of coupled nonlinear partial differential equations (PDEs) describing heat conduction and resin cure kinetics [2, 3]. However, the solution of these PDEs is not available in closed form; computational approximation is required. A popular approach is the finite element method (FEM) [4], which (1) approximates the solution to the PDE at each time point using a collection of

basis functions within discretized sub-domains of the geometry, and (2) iteratively simulates the evolution of the basis function coefficients forward in time. This method has been used to solve the set of governing differential equations for various stages of composite processing such as heat transfer and cure kinetics [2], forming [5, 6], stress development [7, 8], flow analysis [9–11], and most recently in coupled flow-stress analysis [12–15]. However, in situations where repetitive simulations are required—such as optimization, control, real-time monitoring, probabilistic modelling, and uncertainty quantification—the computational cost of the finite element method is prohibitive, as forward simulation involves repeatedly solving large systems of nonlinear equations.

To improve the computational efficiency of simulation, the solution of the PDE can instead be directly approximated using a parametrized function. Once trained, the approximate solution can be evaluated for any given input variables with a fixed computational cost. This approach requires two key components. The first is a parametrized function that is flexible enough to approximate the solution of a complex PDE, but simple enough to be efficiently trained and evaluated. Modern deep neural network (DNN) models [16], which are composed of a sequence of linear transformations and component-wise nonlinearities, provide such functions. DNN models are highly flexible—often having upwards of tens of thousands of parameters—but can still be trained and evaluated efficiently due to recent advances in parallelized hardware, automatic differentiation [17, 18] and stochastic optimization [19].

The remaining key component to this approach is a loss objective which, when minimized, ensures that the parametrized function is a good approximate solution of the PDE. One option is to evaluate a separate high-fidelity model for a collection of inputs, and then to minimize the difference between these values and predictions from the DNN model for the same inputs. This theory-quided machine learning approach [20–23] requires a significant amount of training data from expensive high-fidelity simulations. An alternative approach-Physics-Informed Neural Networks (PINNs) [24]—is to train the DNN model to satisfy the PDE directly at a set of training points, known as sampling or collocation points. By incorporating loss functions based on the PDE, initial condition, and boundary condition residual errors, PINNs recover the solution to the PDE without requiring any other model or simulation. In contrast to early neural network-based differential equation solvers [25– 27, PINNs are trained efficiently using the latest advances of DNNs. A PINN provides numerous advantages over the finite element method: it does not require a mesh-based spatial discretization requiring laborious mesh generation; its derivatives are available once trained; it satisfies the strong form of the differential equations at all training points with known accuracy; and it enables integration of data and mathematical models within same framework [28]. Due to these advantages, many variations of the PINN approach have been successfully used to solve PDEs in a wide range of engineering applications [24, 29–37].

We consider the PINN approach for modelling the thermochemical evolution of a compositetool system during cure. Developing a PINN for this setting presents major challenges. In particular, the system undergoes two simultaneous coupled processes that exhibit very distinct behaviour: the conduction of heat absorbed from the autoclave and generated by the exothermic composite cure process, and the temperature-dependent curing of the composite [2, 3]. Capturing both processes simultaneously in a single PINN is nontrivial both for design and training. Past work on the PINN approach in such multiphysics problems [38] makes use of high-fidelity simulated data—which the PINN method was designed to avoid. Furthermore, the composite-tool system involves a material discontinuity at the composite-tool interface, leading to a discontinuous temperature derivative; standard PINNs [24] produce models with continuous derivatives. While past work has addressed this with domain decomposition [39] on the weak form of the PDEs, it requires separate basis functions within discretized sub-domains of the geometry leading to a multi-element set-up for learning.

In this paper, we propose novel modifications to the PINN approach designed to address the challenges of modelling composite cure in an autoclave. First, we develop an iterative training procedure for decoupled DNNs to model cure and thermal diffusion that mitigates instability present in standard training methods. In addition, we build explicit discontinuities into the DNN at material boundaries, and enforce known boundary behaviour directly in the PINN loss function. We consider the joint composite-tool system, a realistic resin reaction kinetics model [40], and a realistic temperature cycle for the autoclave including heat-up, hold, and cool-down regimes—stages which are all important in determining final residual stresses and part geometry after cure. In concurrent work, Zobeiry and Humfeld [41] developed a PINN to solve the heat transfer PDE in a composite-only system (no tool), without resin reaction kinetics, and for a cure cycle excluding the cool-down regime of the processing. As mentioned above, all of these aspects of the problem are crucial to the realistic simulation of the cure process, and are addressed in the present work.

In the remainder of the paper, we discuss in detail (i) the governing equations for the composite-tool system, (ii) the standard PINN framework, (iii) our proposed modifications to efficiently solve the coupled system of differential equations, (iv) details of an employed adaptive loss weights scheme, and (v) case studies to show the model performance over a range of composite-tool thicknesses.

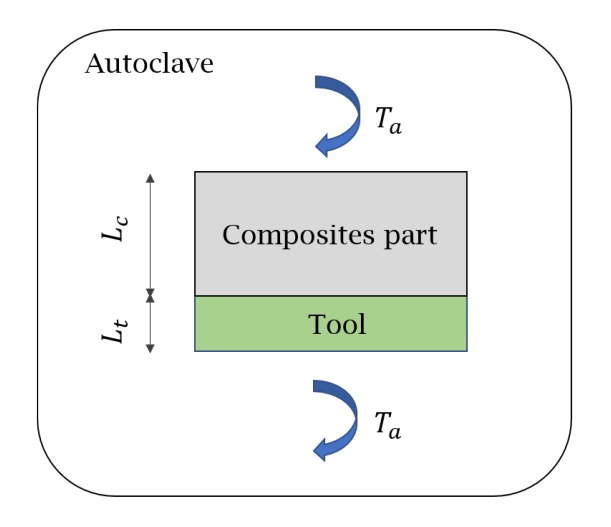
#### 2. Exothermic Heat Transfer in Curing Composite Materials

The exothermic heat transfer in a solid material, i.e. heat transfer with internal heat generation, is governed by the following PDE [2, 3]

$$\frac{\partial}{\partial t} \left( \rho C_p T \right) = \frac{\partial}{\partial x} \left( k_{xx} \frac{\partial T}{\partial x} \right) + \frac{\partial}{\partial y} \left( k_{yy} \frac{\partial T}{\partial y} \right) + \frac{\partial}{\partial z} \left( k_{zz} \frac{\partial T}{\partial z} \right) + \dot{Q}, \tag{1}$$

where T is the temperature,  $C_p$ , k, and  $\rho$  are the specific heat capacity, conductivity, and density of the solid, respectively, and  $\dot{Q}$  is the rate of internal heat generation in the solid. For composite materials with polymeric resin, the internal heat generation is expressed as a function of resin degree of cure  $\alpha \in (0,1)$ , which is a measure of the conversion achieved during crosslinking reactions of the resin material [2]. In particular, the relationship between  $\dot{Q}$  and  $\alpha$  may be expressed as

$$\dot{Q} = \nu_r \rho_r H_r \frac{d\alpha}{dt},\tag{2}$$



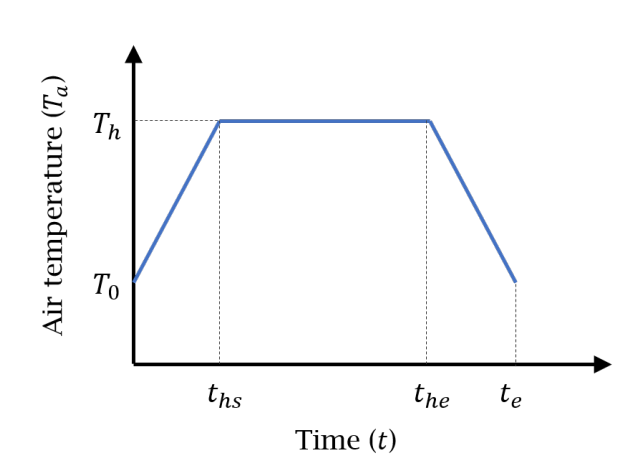


Figure 1: (Left) A schematic of composite-tool material system inside an autoclave; (Right) autoclave air temperature history during the processing time.

where subscript r represents resin,  $\nu$  is volume fraction, and H is the heat of reaction generated per unit mass of resin during curing. Considering a one-dimensional system with homogeneous material, i.e.  $\frac{\partial k}{\partial x} = 0$ , with temperature-independent physical properties, i.e.  $\frac{\partial \rho}{\partial t} = \frac{\partial C_p}{\partial t} = 0$ , we can rewrite Eq. (1) as

$$\frac{\partial T}{\partial t} = a \frac{\partial^2 T}{\partial x^2} + b \frac{d\alpha}{dt} \quad \text{where} \quad a = \frac{k}{\rho C_p} \quad \text{and} \quad b = \frac{\nu_r \rho_r H_r}{\rho C_p}. \tag{3}$$

In polymeric composite materials, the evolving degree of cure  $\alpha$  is typically governed by an ordinary differential equation that expresses the rate of cure as a function of instantaneous temperature and degree of cure,

$$\frac{d\alpha}{dt} = g(\alpha, T). \tag{4}$$

This leads to a coupled system of differential equations (Eqs. (3) and (4)) for temperature and degree of cure in the space-time domain, (x,t). Solution of this system of differential equations subjected to initial and boundary conditions results in predictions of temperature T(x,t) and degree of cure  $\alpha(x,t)$  in the composite material.

In this study, we focus on solving the system of differential equations for the compositetool system shown in Fig. 1. Heat transfer in this bi-material system is governed by the differential equations (3) and (4). However, the material properties are discontinuous at the intersection point of the composite and the tool material,  $x = L_t$ , i.e.

$$a = \begin{cases} a_t & \text{for} & 0 < x < L_t \\ a_c & \text{for} & L_t < x < L_t + L_c \end{cases},$$

$$b = \begin{cases} 0 & \text{for} & 0 < x < L_t \\ b_c & \text{for} & L_t < x < L_t + L_c \end{cases},$$

$$(5)$$

where the subscripts c and t represent composite and tool materials, respectively. In an autoclave the air temperature,  $T_a$ , evolves over time during processing; an example is shown in Fig. 1. Therefore, the boundary conditions at both ends can be specified to be equal to the autoclave air temperature (prescribed boundary conditions) via

$$T|_{x=0} = T_a(t),$$
  
 $T|_{x=L_t+L_c} = T_a(t).$  (6)

However, we may instead capture a more realistic assumption that heat transfers between the air inside the autoclave and the solid materials within it (*convective* boundary conditions) via

$$h_t \left( T|_{x=0} - T_a(t) \right) = k_t \frac{\partial T}{\partial x}|_{x=0},$$

$$h_c \left( T_a(t) - T|_{x=L_t+L_c} \right) = k_c \frac{\partial T}{\partial x}|_{x=L_t+L_c},$$
(7)

where h is the convective heat transfer coefficient at the interface between the air and the solid. The initial conditions are expressed as

$$T|_{t=0} = T_0(x),$$
  
 $\alpha|_{t=0} = \alpha_0(x),$ 
(8)

where  $T_0$  is the initial temperature of the system, usually considered constant for the entire geometry, and  $\alpha_0$  is the resin initial degree of cure which is considered zero (or a very small number) for uncured resin material over the entire spatial domain.

#### 3. Physics-Informed Neural Network for Thermochemical Cure Process

In this section, we first develop the physics-informed neural network (PINN) formulation for heat transfer in a single material with internal heat generation. Subsequently, we extend the formulation for the more practical composite-tool material system shown in Fig. 1.

#### 3.1. PINN for a single material system

In our heat transfer formulation presented in the previous section,  $\boldsymbol{x} := (x,t)$  is introduced as the set of independent space and time variables (x,t) and  $\boldsymbol{y} := (T,\alpha)$  represents the set of dependent temperature and degree of cure solution variables  $(T,\alpha)$ . Based on the PINN framework [24], the solution variable  $\boldsymbol{y}$  is approximated using a feed-forward multi-layer neural network

$$y(x) \approx \mathcal{N}(x; \theta),$$
 (9)

where  $\mathcal{N}$  is an  $\Lambda$ -layer neural network with input features  $\boldsymbol{x}=(x,t)$  and set of all network parameters  $\boldsymbol{\theta} \in \mathbb{R}^D$ , where D is the total number of parameters (equivalent to the total number of degrees of freedom in the FEM sense). A schematic of the network for standard PINN is shown in Fig. 2. Analytically, this network represents the following compositional function

$$\mathcal{N}(\boldsymbol{x};\boldsymbol{\theta}) = \Sigma^{\Lambda} \circ \Sigma^{\Lambda-1} \circ \cdots \circ \Sigma^{1}(\boldsymbol{x}), \tag{10}$$

# 

Figure 2: A schematic of a single neural network architecture with space and time input features (x,t) and degree of cure and temperature outputs  $(\alpha,T)$  with a multi-objective optimization of the total loss function consisted of loss terms for governing equations, initial, and boundary conditions.

where

$$\Sigma^{\lambda}(\boldsymbol{z}^{\lambda-1}) := \boldsymbol{z}^{\lambda} = \sigma^{\lambda}(\mathbf{W}^{\lambda} \cdot \boldsymbol{z}^{\lambda-1} + \mathbf{b}^{\lambda}) \quad \text{where} \quad \lambda = 1, ..., \Lambda.$$
 (11)

In the above equations, the symbol  $\circ$  denotes the composition operation, superscript  $\lambda$  is the layer number,  $\mathbf{z}^0 := \mathbf{x}$  are the inputs (x,t) to the network,  $\mathbf{z}^{\Lambda} := \mathbf{y}$  are the outputs  $(T,\alpha)$  of the network, and  $\mathbf{W}^{\lambda}$  and  $\mathbf{b}^{\lambda}$  are the parameters of layer  $\lambda$ , also known as weight matrices and bias vectors, all collected in  $\boldsymbol{\theta}$ .  $\sigma^{\lambda}$  are so-called activation functions which introduce nonlinearity into the neural network [42]. Typically a single function—such as the hyperbolic-tangent function—is selected for all layers except for the last layer,  $\sigma^{\Lambda}$ , which is selected based on the output variables, here T and  $\alpha$ .

If the activation function  $\sigma$  is continuous and differentiable, the neural network in Eq. (10) will have these properties over the  $\boldsymbol{x}$  domain as well. In PINNs, an error or loss function is defined using the processed outputs of the network and their derivatives based on the equations governing the physics of the problem. In particular for our problem, the total loss of the network,  $\mathcal{L}_{\mathcal{N}}$ , consists of the sum of loss terms for the PDE ( $\mathcal{L}_{\alpha}$  and  $\mathcal{L}_{T}$ ), the initial conditions ( $\mathcal{L}_{\alpha_0}$  and  $\mathcal{L}_{T_0}$ ), and the boundary conditions ( $\mathcal{L}_{T_{bc_1}}$  and  $\mathcal{L}_{T_{bc_2}}$ ),

$$\mathcal{L}_{\mathcal{N}} = \mathcal{L}_{\alpha} + \mathcal{L}_{T} + \mathcal{L}_{\alpha_0} + \mathcal{L}_{T_0} + \mathcal{L}_{T_{bc_1}} + \mathcal{L}_{T_{bc_2}}, \tag{12}$$

where each term is evaluated on a set of training or *collocation* points in the domain denoted as X. The PDE losses associated with Eqs. (3) and (4), in the form of mean squared error

terms, are expressed as

$$\mathcal{L}_{\alpha} = \frac{1}{n} \sum_{i=1}^{n} \left( \frac{d\alpha}{dt} |_{\boldsymbol{x}_{i}} - g(\alpha, T)|_{\boldsymbol{x}_{i}} \right)^{2},$$

$$\mathcal{L}_{T} = \frac{1}{n} \sum_{i=1}^{n} \left( \frac{\partial T}{\partial t} |_{\boldsymbol{x}_{i}} - a \frac{\partial^{2} T}{\partial x^{2}} |_{\boldsymbol{x}_{i}} - b \frac{d\alpha}{dt} |_{\boldsymbol{x}_{i}} \right)^{2},$$
(13)

where n is the total number of collocation points and  $x_i \in \mathbf{X}$ . For the case of prescribed temperature boundary conditions, the losses associated with initial and boundary conditions Eqs. (6) and (8) are defined as

$$\mathcal{L}_{\alpha_0} = \frac{1}{n} \sum_{i=1}^{n} \left( \alpha |_{t=0} - \alpha_0(x) \right)^2,$$

$$\mathcal{L}_{T_0} = \frac{1}{n} \sum_{i=1}^{n} \left( T |_{t=0} - T_0(x) \right)^2,$$

$$\mathcal{L}_{T_{bc_1}} = \frac{1}{n} \sum_{i=1}^{n} \left( T |_{x=0} - T_a(t) \right)^2,$$

$$\mathcal{L}_{T_{bc_2}} = \frac{1}{n} \sum_{i=1}^{n} \left( T |_{x=L_t + L_c} - T_a(t) \right)^2.$$
(14)

For the convective heat transfer boundary condition expressed in Eq. (7), the last two terms in the above equation, i.e.  $\mathcal{L}_{T_{bc_1}}$  and  $\mathcal{L}_{T_{bc_2}}$ , are replaced with

$$\mathcal{L}_{T_{bc_1}} = \frac{1}{n} \sum_{i=1}^{n} \left( h_t \left( T|_{x=0} - T_a(t) \right) - k_t \frac{\partial T}{\partial x}|_{x=0} \right)^2, 
\mathcal{L}_{T_{bc_2}} = \frac{1}{n} \sum_{i=1}^{n} \left( h_c \left( T_a(t) - T|_{x=L_t+L_c} \right) - k_c \frac{\partial T}{\partial x}|_{x=L_t+L_c} \right)^2.$$
(15)

The network is then trained by minimizing the total loss for the set of network parameters  $\theta$  at the collocation points X,

$$\boldsymbol{\theta}^* = \operatorname*{argmin}_{\boldsymbol{\theta} \in \mathbb{R}^D} \mathcal{L}_{\mathcal{N}}(\mathbf{X}; \ \boldsymbol{\theta}). \tag{16}$$

It is worth noting that the loss terms include derivatives of the DNN function approximations of T and  $\alpha$ ; it is possible to compute these exactly using automatic differentiation [18] at any point in the domain without the need for manual computation.

However, given the coupling of  $\mathcal{L}_{\alpha}$  and  $\mathcal{L}_{T}$  loss terms in Eq. (13), training a single network for both  $\alpha$  and T outputs is not straightforward. For example, Fig. 3 (left) shows that standard minimization algorithms fail to reduce the losses associated with the  $\alpha$  output to an acceptable level. Here we take inspiration from classical solution methods (e.g., FEM), where

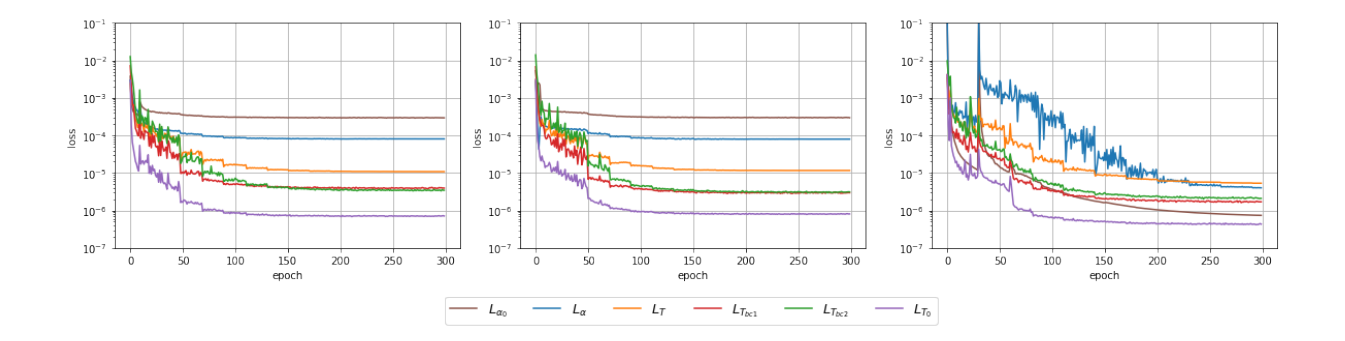


Figure 3: Evolution of different loss terms in the training of the network. (Left) A joint network architecture, 5 layers and 42 nodes (7436 parameters in total); (Middle) a disjoint network architecture with simultaneous training, 5 layers and 30 nodes for each network (7682 parameters in total); (Right) a disjoint network architecture with the proposed sequential training procedure, 5 layers and 30 nodes for each network (7682 parameters in total).

each output is approximated independently without sharing degrees of freedom. Rather than a single network, we train two separate networks—one for each output variable,  $\alpha$  and T—in a manner that resembles past disjoint PINNs [37, 38, 43, 44],

$$\alpha(\mathbf{x}) \approx \mathcal{N}_{\alpha}(\mathbf{x}; \; \boldsymbol{\theta}_{\alpha}),$$

$$T(\mathbf{x}) \approx \mathcal{N}_{T}(\mathbf{x}; \; \boldsymbol{\theta}_{T}),$$
(17)

where  $\boldsymbol{\theta}_{\alpha} \in \mathbb{R}^{D_{\alpha}}$  and  $\boldsymbol{\theta}_{T} \in \mathbb{R}^{D_{T}}$  are the parameters for the individual networks. In addition, even with separate networks, simultaneous training of both networks also tends to fail as demonstrated in Fig. 3 (middle). To resolve this, we propose the use of sequential training for  $\alpha$  and T. In particular, we first optimize the network parameters of  $\mathcal{N}_{\alpha}$  with those of  $\mathcal{N}_{T}$  fixed, then vice versa, and the process is iterated until convergence is achieved. In this sequential approach, the total loss in Eq. (12) is then decoupled as

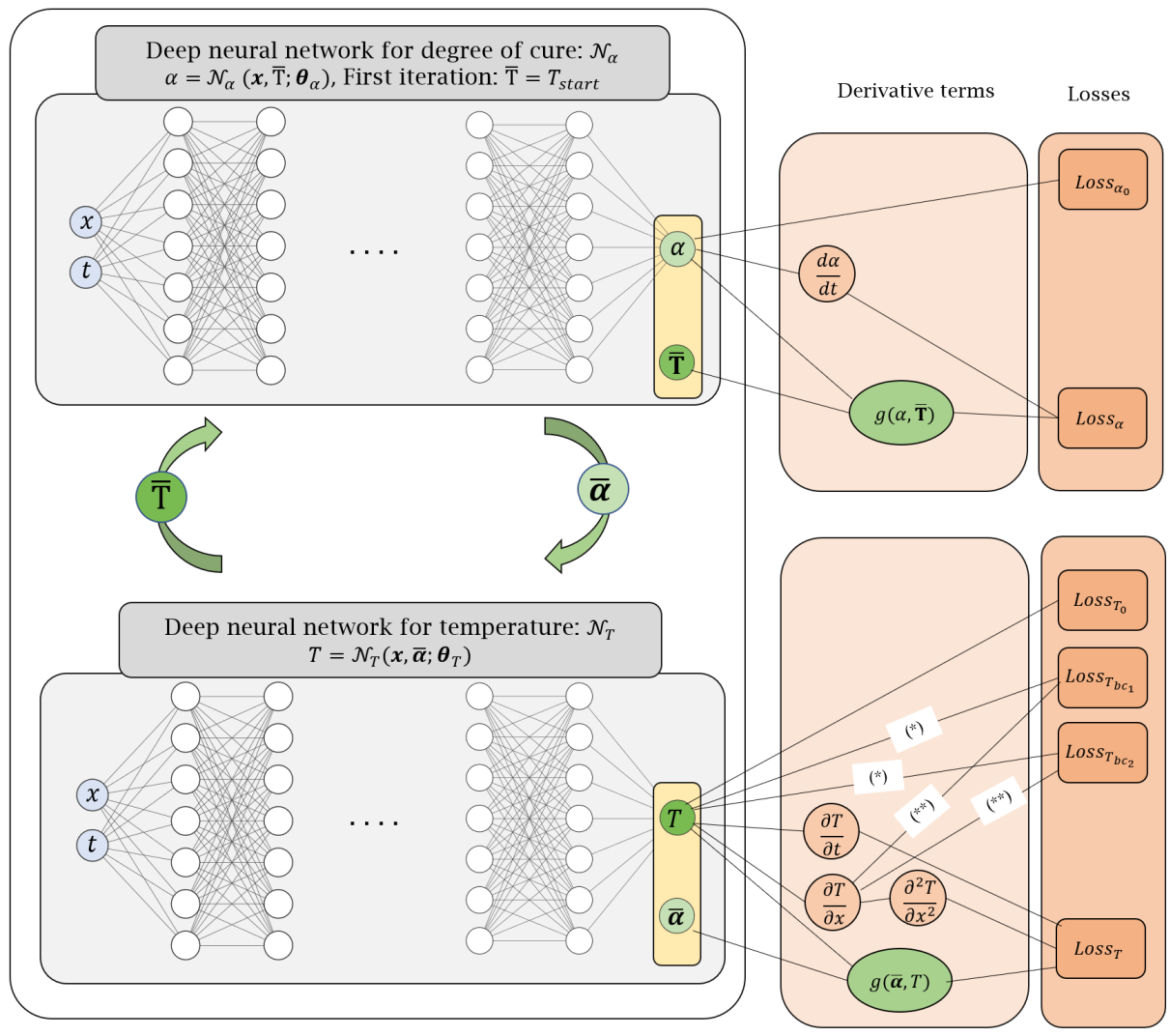
$$\mathcal{L}_{\mathcal{N}_{\alpha}} = \mathcal{L}_{\alpha} + \mathcal{L}_{\alpha_{0}},$$

$$\mathcal{L}_{\mathcal{N}_{T}} = \mathcal{L}_{T} + \mathcal{L}_{T_{0}} + \mathcal{L}_{T_{bc_{1}}} + \mathcal{L}_{T_{bc_{2}}}.$$
(18)

The optimization problem for the jth iteration of sequential training, with initial network parameters  $\theta_{\alpha}^{*j}$  and  $\theta_{T}^{*j}$ , is defined as

$$\theta_{\alpha}^{*j+1} = \underset{\boldsymbol{\theta}_{\alpha} \in \mathbb{R}^{D_{\alpha}}}{\operatorname{argmin}} \mathcal{L}_{\mathcal{N}_{\alpha}}(\mathbf{X}, \bar{\mathbf{T}}^{j}; \boldsymbol{\theta}_{\alpha}), 
\boldsymbol{\theta}_{T}^{*j+1} = \underset{\boldsymbol{\theta}_{T} \in \mathbb{R}^{D_{T}}}{\operatorname{argmin}} \mathcal{L}_{\mathcal{N}_{T}}(\mathbf{X}, \bar{\boldsymbol{\alpha}}^{j+1}; \boldsymbol{\theta}_{T}), \tag{19}$$

with  $\bar{\boldsymbol{\alpha}}^j = \mathcal{N}_{\alpha}(\mathbf{X}; \boldsymbol{\theta}_T^{*j})$  and  $\bar{\mathbf{T}}^j = \mathcal{N}_T(\mathbf{X}; \boldsymbol{\theta}_{\alpha}^{*j})$  as the sequentially approximated values of solution variables in Eq. (17) on the training points  $\mathbf{X}$ . A schematic architecture of the proposed network and the sequential training procedure is shown in Fig. 4. The convergence of the various losses in the proposed PINN using the proposed sequential training procedure



- (\*) For prescribed temperature boundary condition
- (\*\*) For convective boundary condition

Figure 4: A schematic of network architecture for a single material system. Two separate networks are constructed for T and  $\alpha$  with sequential training first on  $\alpha$ , and then on T, until convergence.

and decoupled networks for  $\alpha$  and T also is illustrated in Fig. 3 (right). In this figure, the  $\alpha$ -related losses are trained for 30 epochs, then the T-related losses for 30 epochs, and this is repeated for 10 iterations. The sequential procedure successfully reduces all loss terms to a level below  $10^{-5}$ .

# 3.2. PINN for a bi-material system

By construction, the feed-forward multi-layer neural network (9) (and both networks in Eq. (17)) with a differentiable activation function, e.g. hyperbolic-tangent, represents a continuous and differentiable function in space and time for any given  $\boldsymbol{x}$  in the domain.

However, for a bi-material system where the material properties are discontinuous at the interface, the derivative of solution variables is discontinuous at that point. To improve the accuracy of the neural network approximations for problems where we expect such discontinuous solutions at the bi-material interface  $x = x_I$ , where  $x_I = L_t$  in Fig. 1, we propose the following construction for both neural networks  $\mathcal{N}_{\alpha}$  and  $\mathcal{N}_T$ :

$$\mathcal{N}(\boldsymbol{x};\boldsymbol{\theta}) = H(x_I - x)\mathcal{N}^-(\boldsymbol{x}; \boldsymbol{\theta}^-) + H(x - x_I)\mathcal{N}^+(\boldsymbol{x}; \boldsymbol{\theta}^+), \tag{20}$$

where H is the heaviside step function defined as

$$H(x) = \begin{cases} 1 & \text{if } x \ge 0\\ 0 & \text{if } x < 0. \end{cases}$$
 (21)

This construction of a neural network using two components  $\mathcal{N}^-$  and  $\mathcal{N}^+$  with distinct parameters  $\boldsymbol{\theta}^-$  and  $\boldsymbol{\theta}^+$ , implies that the space of possible solutions for  $\boldsymbol{y} \approx \mathcal{N}(\boldsymbol{x}; \boldsymbol{\theta})$  and its spatial derivative can be discontinuous at  $x = x_I$ , i.e.

$$\mathbf{y}|_{x^{+}} - \mathbf{y}|_{x^{-}} = \mathcal{N}^{+}(\mathbf{x}; \; \boldsymbol{\theta}^{+}) - \mathcal{N}^{-}(\mathbf{x}; \; \boldsymbol{\theta}^{-}),$$

$$\frac{\partial \mathbf{y}}{\partial x}|_{x^{+}} - \frac{\partial \mathbf{y}}{\partial x}|_{x^{-}} = \frac{\partial \mathcal{N}^{+}(\mathbf{x}; \; \boldsymbol{\theta}^{+})}{\partial x} - \frac{\partial \mathcal{N}^{-}(\mathbf{x}; \; \boldsymbol{\theta}^{-})}{\partial x}.$$
(22)

Therefore, the functional form (20) can approximate discontinuous solution at  $x = x_I$ .

For the bi-material composite-tool system, the degree of cure is only applicable to the composite material. The temperature distribution, however, is defined for both the tool and the composite part. Following the previous discussions on the choice of networks, the solution space in Eq. (17) is then defined as

$$\alpha(\boldsymbol{x}) \approx H(x - x_I) \mathcal{N}_{\alpha}^{+}(\boldsymbol{x}; \; \boldsymbol{\theta}_{\alpha}^{+}),$$

$$T(\boldsymbol{x}) \approx H(x_I - x) \mathcal{N}_{T}^{-}(\boldsymbol{x}; \; \boldsymbol{\theta}_{T}^{-}) + H(x - x_I) \mathcal{N}_{T}^{+}(\boldsymbol{x}; \; \boldsymbol{\theta}_{T}^{+}),$$
(23)

which is schematically shown in Fig. 5 where the  $T^-$  and  $T^+$  nodal values are

$$T^{-} = \mathcal{N}_{T}^{-}(\boldsymbol{x}; \; \boldsymbol{\theta}_{T}^{-}),$$

$$T^{+} = \mathcal{N}_{T}^{+}(\boldsymbol{x}; \; \boldsymbol{\theta}_{T}^{+}).$$
(24)

At the interface point between the tool and the composite, i.e. at  $x=x_I$ , the temperature field should remain continuous. However, as shown in Eq. (22), the temperature from the neural network is allowed to be discontinuous. Therefore, the optimization should satisfy  $T|_{x=x_I^+} - T|_{x=x_I^-} = 0$  in order to impose the continuity condition for the temperature. Additionally, although the spatial derivative  $\frac{\partial T}{\partial x}$  may be discontinuous, the heat conservation implies that the heat flux across the interface should also be continuous, i.e.,  $k^+ \frac{\partial T^+}{\partial x}|_{x=x_I} - k^- \frac{\partial T^-}{\partial x}|_{x=x_I} = 0$ . The loss terms for these two conditions are expressed as

$$\mathcal{L}_{\tau} = \sum_{i=1}^{n} \left( T^{+}|_{x=x_{I}} - T^{-}|_{x=x_{I}} \right)^{2},$$

$$\mathcal{L}_{q} = \sum_{i=1}^{n} \left( k^{+} \frac{\partial T^{+}}{\partial x}|_{x=x_{I}} - k^{-} \frac{\partial T^{-}}{\partial x}|_{x=x_{I}} \right)^{2},$$
(25)

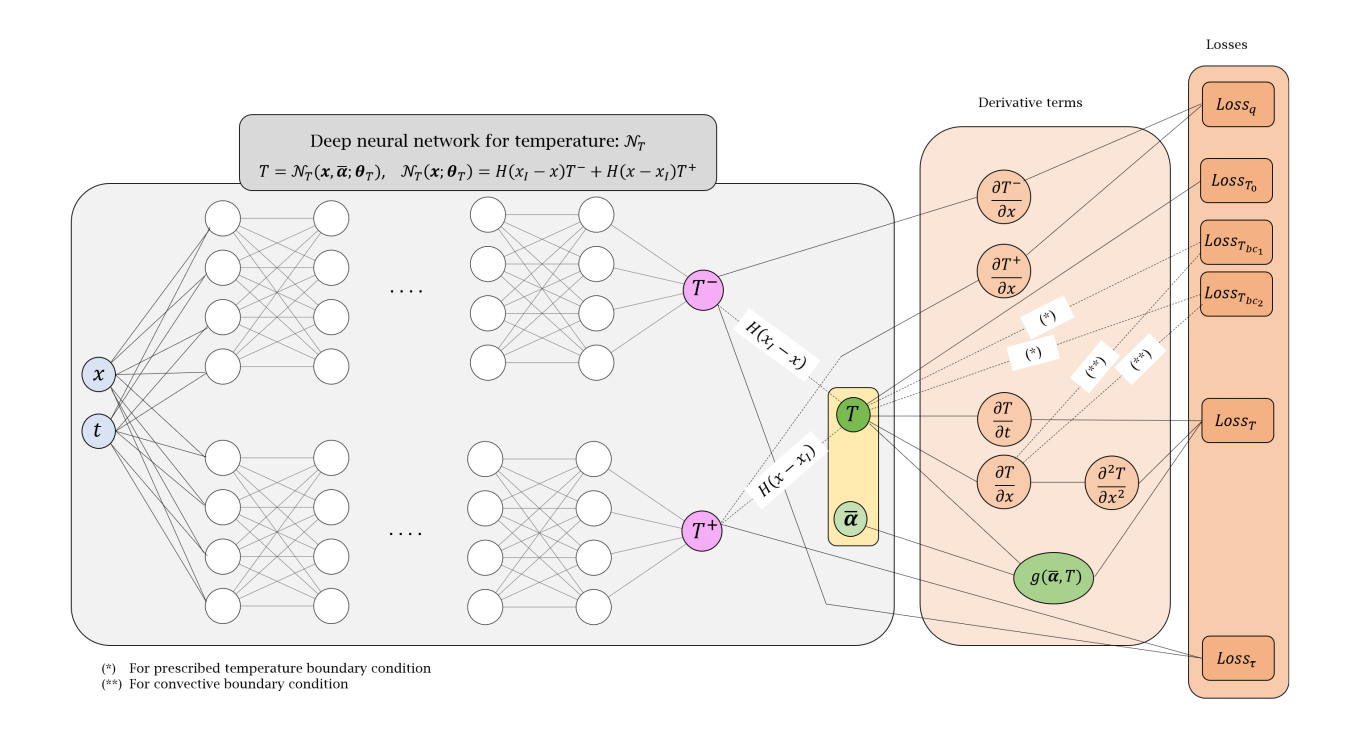


Figure 5: A schematic of a discontinuous network architecture utilized for the bi-material problem. Two separate networks  $T^-$  and  $T^+$  are combined with Heaviside step function H to construct the solution space for T.

where  $k^-$  and  $k^+$  are  $k_t$  and  $k_c$ , respectively, and  $x_I = L_t$  in the composite-tool setup in Fig. 1. Based on the cases we studied, this choice of network is contributing strongly to accurate modeling of the bi-material composite-tool system.

# 3.3. Network and optimization hyper-parameters

For training of PINN described above, it is crucial to use activation functions tailored to the underlying differential equations and the physical output quantities. Using physics based rationale, an activation function with positive output parameter and non-zero derivative (which is important in physics based neural networks) is an obvious choice for the last layer of  $\mathcal{N}_T$ . Therefore, in order to result in a positive absolute temperature T > 0, the Softplus function is used which is defined as

$$Softplus(x) = \ln(1 + e^x). \tag{26}$$

For the degree of cure, which is defined in  $\alpha \in (0,1)$ , the *Sigmoid* function is a natural choice for the last layer of  $\mathcal{N}_{\alpha}$  where its following modified version is used in those cases where curing of the composite starts from a nonzero value,  $\alpha_0$ ,

Sigmoid'(x) = 
$$\frac{1 - \alpha_0}{1 + e^{-x}} + \alpha_0$$
. (27)

For all hidden layers, hyperbolic-tangent function is used which is a preferable activation function due to its smoothness and non-zero derivative.

#### 3.4. Adaptive loss weights

As discussed by others [24], training the multi-objective total loss functions, e.g.  $\mathcal{L}_{\mathcal{N}_{\alpha}}$  and  $\mathcal{L}_{\mathcal{N}_{T}}$  in Eq. (18), poses challenges for optimization techniques. Particularly for boundary value problems, the unique solution to the governing equations is achieved when initial and boundary conditions are imposed strongly. Within the context of multi-objective optimization, a weighted-sum scheme is commonly employed to improve the optimization algorithms [45]. In practice, the loss weights are often tuned manually in a very tedious trial-and-error procedure based on the convergence analysis of the optimization process. Within the context of PINNs, Wang et al. [46] showed that inaccuracy in optimization is particularly affected by unbalanced gradients and proposed an adaptive loss weight algorithm based on normalizing the gradient of individual terms in the loss function in order to reduce the stiffness of the gradient flow dynamics. Therefore, the total loss terms  $\mathcal{L}_{\mathcal{N}_{\alpha}}$  and  $\mathcal{L}_{\mathcal{N}_{T}}$  in Eq. (18) are modified as

$$\mathcal{L}_{\mathcal{N}_{\alpha}} = \mathcal{L}_{\alpha} + \omega_{\alpha_0} \mathcal{L}_{\alpha_0},$$

$$\mathcal{L}_{\mathcal{N}_{T}} = \mathcal{L}_{T} + \omega_{T_0} \mathcal{L}_{T_0} + \omega_{T_{bc_1}} \mathcal{L}_{T_{bc_1}} + \omega_{T_{bc_2}} \mathcal{L}_{T_{bc_2}},$$
(28)

where  $\omega$  denotes the loss weight corresponding to each loss term. The updated scaling weight  $\omega^{e+1}$  for each loss term is evaluated based on the parameter values  $\theta^e$  at epoch e as

$$\omega^{e+1} = \beta \omega^e + (1 - \beta)\hat{\omega}^{e+1},\tag{29}$$

where

$$\hat{\omega}_{\alpha_0}^{e+1} = \frac{1}{\omega_{\alpha_0}^e} \frac{\max(|\nabla_{\theta} \mathcal{L}_{\alpha}(\boldsymbol{\theta}^e)|)}{\max(|\nabla_{\theta} \mathcal{L}_{\alpha_0}(\boldsymbol{\theta}^e)|)} \quad \text{for } \mathcal{N}_{\alpha},$$

$$\hat{\omega}_i^{e+1} = \frac{1}{\omega_i^e} \frac{\max(|\nabla_{\theta} \mathcal{L}_T(\boldsymbol{\theta}^e)|)}{\max(|\nabla_{\theta} \mathcal{L}_I(\boldsymbol{\theta}^e)|)} \quad \text{for } \mathcal{N}_T, \quad \text{where } i \in \{T_0, T_{bc_1}, T_{bc_2}\}.$$
(30)

In the above equation,  $\nabla_{\theta}$  shows gradient of the loss with respect to the parameter of the network and  $\beta$  is taken as 0.9. Note that relations Eqs. (29) and (30) are based on the actual implementation shared by the authors, that are slightly different from the reported relations by Wang et al. [46]. The loss weight updates could be performed at every epoch or at a frequency specified by the user [46]. Such adaptive method for loss weights enhances robustness of the method and leads to improvement in accuracy of the model predictions.

#### 4. Case studies

To check the performance of the proposed PINN, the exothermic heat transfer in a AS4/8552 composite part on an Invar tool is modelled. The resin reaction in 8552 epoxy follows a cure kinetics differential equation presented in [40] as

$$\frac{\mathrm{d}\alpha}{\mathrm{d}t} = \frac{A \exp\left(\frac{-\Delta E}{RT}\right)}{\exp\left(C\left(\alpha - C_T T - C_0\right)\right)} \alpha^M (1 - \alpha)^N,\tag{31}$$

where the right hand side of the equation represents  $g(\alpha, T)$ . All parameters in Eq. (31) are listed in Table 1 along with material properties for AS4 fibre, 8552 epoxy resin, and Invar

Parameter	Value
A (1/s)	$1.528 \times 10^{5}$
$\Delta E \text{ (J/mol)}$	$6.650 \times 10^4$
M	0.8129
N	2.7360
C	43.09
$C_0$	-0.6840
$C_T (1/K)$	$5.475 \times 10^{-3}$
R (J/mol K)	8.314

Table 1: Parameters for resin 8552 cure kinetics model in Eq. 23.

Matarial parameter	AS4 fibre	8552 resin [40]	Invar tool
Material parameter	(f)	(r)	$  \qquad  $
Volume fraction, $\nu$	0.574	0.426	-
Density, $\rho$ (kg/m <sup>3</sup> )	1790	1300	8150
Conductivity, $k$ (W/m K)	3.960	0.212	13.0
Specific heat capacity, $C_p$ (J/kg K)	914.0	1304.2	510.0

Table 2: Thermal material properties of fibre, resin, and tool.

tool in Table 2. The composite properties in the transverse direction, i.e. through thickness, are obtained from those of the fibre and resin [40, 47] as

$$\rho_c = \rho_r \nu_r + \rho_f \nu_f, 
C_{p_c} = C_{p_r} \nu_r + C_{p_f} \nu_f, 
k_c = k_r \left( (1 - 2\Omega) + \frac{1}{\Omega} \left( \pi - \frac{4}{\Upsilon} \tan^{-1} \left( \frac{\Upsilon}{1 + \Omega \Gamma} \right) \right) \right),$$
(32)

where

$$\Gamma = 2\left(\frac{k_r}{k_f} - 1\right),$$

$$\Omega = \sqrt{\frac{\nu_f}{\pi}},$$

$$\Upsilon = \sqrt{1 - \Gamma^2 \Omega^2}.$$
(33)

Results are presented for four case studies with different boundary conditions and different lengths of the composite and the tool, as listed in Table 3. For cases 1 and 2, the thickness of composite is  $L_c = 30 \,\mathrm{mm}$  which sits on a  $L_t = 20 \,\mathrm{mm}$  tool, while for cases 3 and 4, they are taken as  $L_c = 300 \,\mathrm{mm}$  and  $L_t = 200 \,\mathrm{mm}$ . Cases 1 and 3 are subjected to prescribed temperature at the boundary while cases 2 and 4 are subjected to convective boundary conditions. For all cases, the autoclave air temperature follows a heat up-hold-cool down cycle as shown in Fig. 1 with  $T_0 = 293 \,\mathrm{K}(20\,^{\circ}\mathrm{C})$ ,  $T_h = 453 \,\mathrm{K}(180\,^{\circ}\mathrm{C})$ ,  $t_{hs} = 52 \,\mathrm{min}$ ,  $t_{he} = 172 \,\mathrm{min}$ , and  $t_e = 222 \,\mathrm{min}$ . The initial temperature of both composite and tool are

Case study	Boundary condition	Length	Section number
J	$(K \text{ or } W/m^2K)$	(mm)	in the paper
Case 1	Prescribed temperature		
Case 1	$T_{bc_1} = T_a(t) \text{ and } T_{bc_2} = T_a(t)$	$L_t = 20$	Section 4
Case 2	Convective	$L_c = 30$	Decilon 4
Case 2	$h_t = 70 \text{ and } h_c = 120$		
Case 3	Prescribed temperature		
Case 3	$T_{bc_1} = T_a(t) \text{ and } T_{bc_2} = T_a(t)$	$L_t = 200$	Appendix A
Case 4	Convective	$L_c = 300$	Appendix A
Case 4	$h_t = 70 \text{ and } h_c = 120$		

Table 3: Length and boundary conditions for different case studies.

prescribed as  $T_0 = 293 \,\mathrm{K}$ . The training is conducted on a uniform grid with 500 points on  $0 < x < L_t + L_c$  and 1,000 points on  $0 < t < t_e$  Additionally, we use, 10,000 uniformly distributed points in (x, t = 0) as well as 5,000 points on each of (x = 0, t) and  $(x = L_t + L_c, t)$ to enforce the initial and the two boundary conditions. Any graph-based framework such as Theano [17], Tensorflow [48], or PyTorch [49], or high-level Application Programming Interfaces (API) of these platforms, such as Keras [50], used in this work, can be employed to efficiently construct the network and perform the optimization. There are also APIs, such as DeepXDE [51] or SciANN [52], that are specifically designed for setting up and training PINN models. We design a fully connected neural network to have 7 hidden layers and 30 nodes per layer (5701 parameters in total) for  $\mathcal{N}_{\alpha}$ , shown in Fig. 4. For the temperature networks  $\mathcal{N}_T^-$  and  $\mathcal{N}_T^+$ , Eq. (23) and Fig. 5, again we pick 7 layers with 20 nodes per layer for each networks (5202 parameters in total). A mini-batch optimization with a batch size of 512 is used employing the Adam optimizer [53], which is based on the stochastic gradient descent. A learning rate scheduler is also used for the optimization starting from  $10^{-3}$  and reducing by a factor of 0.5 in case there are no improvement in the total loss values after 20 and 10 epochs for temperature and degree of cure, respectively. The analysis is performed for 10 iterations with 30 epochs for each of  $\alpha$  and T in each iteration, i.e. 300 total epochs of training for each of  $\mathcal{N}_{\alpha}$  and  $\mathcal{N}_{T}$ . The adaptive loss weight algorithm is also applied to both  $\mathcal{N}_{\alpha}$  and  $\mathcal{N}_{T}$  where loss weights are updated at the beginning of each iteration of training of each network, rather than each each training epoch, for reducing the computational cost of training.

# 4.1. Predictions of temperature and degree of cure

To check the accuracy of the PINN method in prediction of T and  $\alpha$  field variables, results are compared against FE predictions from RAVEN 3.13.1 [54] software. The temperature and degree of cure predictions for case studies 1 and 2 are shown in Figs. 6 and 7. The relative percentage error of the predicted temperature between PINN and FEM is less than 1%. In Figs. 8 and 9, the temperature evolution at the bottom of the tool, composite-tool intersection, middle of the composite material, and top of the composite are shown for the full cure cycle. PINN accurately captures the maximum part temperature, i.e. exotherm,

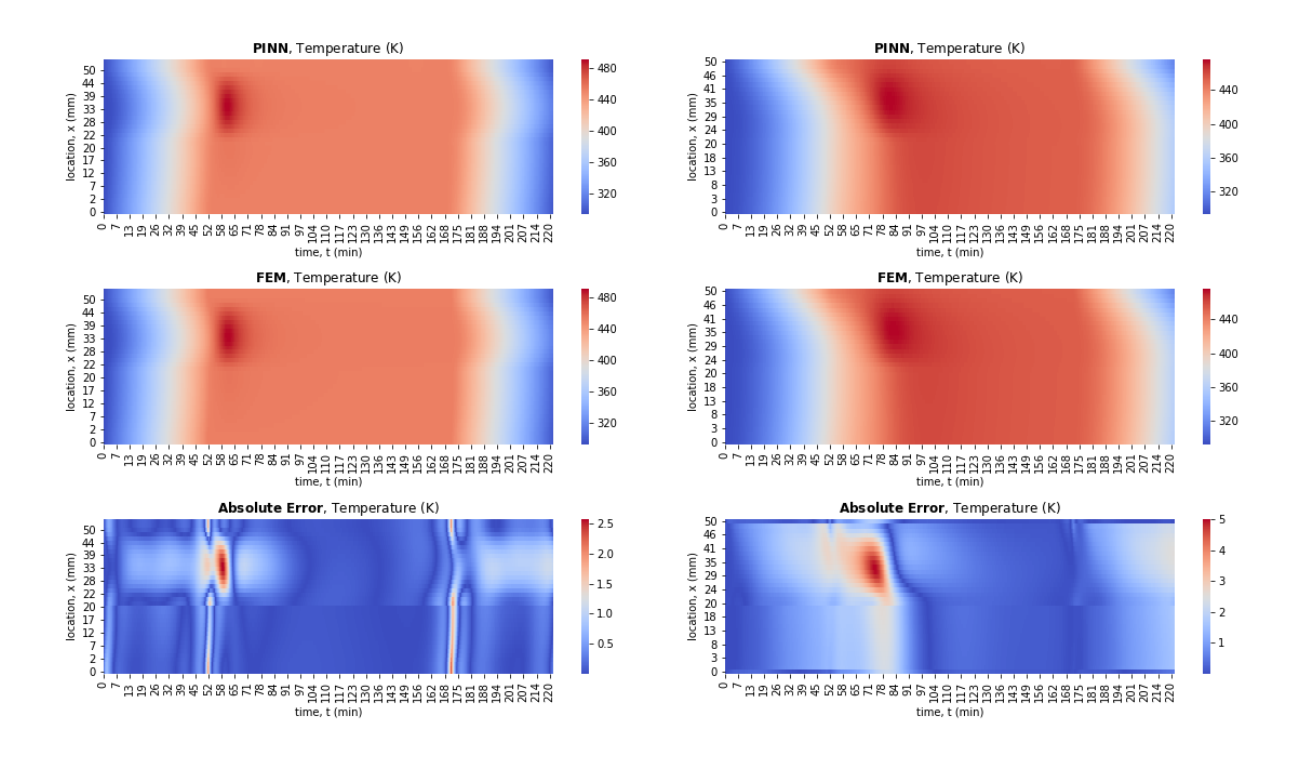


Figure 6: PINN and FEM temperature predictions for (Left) case study 1 and (Right) case study 2.

that occurs at the middle of the composite part due to internal heat generated from resin reaction. For case study 1, equality of the tool and composite temperature at the boundary of the autoclave air temperature is captured accurately. For the case study 2, the temperature at the boundaries lags behind the air temperature due to convective heat transfer, known as thermal lag. Due to lower convective heat transfer coefficient, h, for the tool material, the thermal lag is more pronounced compared to the composite. Accurate predictions of both the exotherm and thermal lag are of great importance in processing of composite materials inside autoclaves. To further check the performance of the model, an extreme and unrealistic case involving  $L_c = 300 \,\mathrm{mm}$  and  $L_t = 200 \,\mathrm{mm}$  is also performed the results of which are presented in Appendix A.

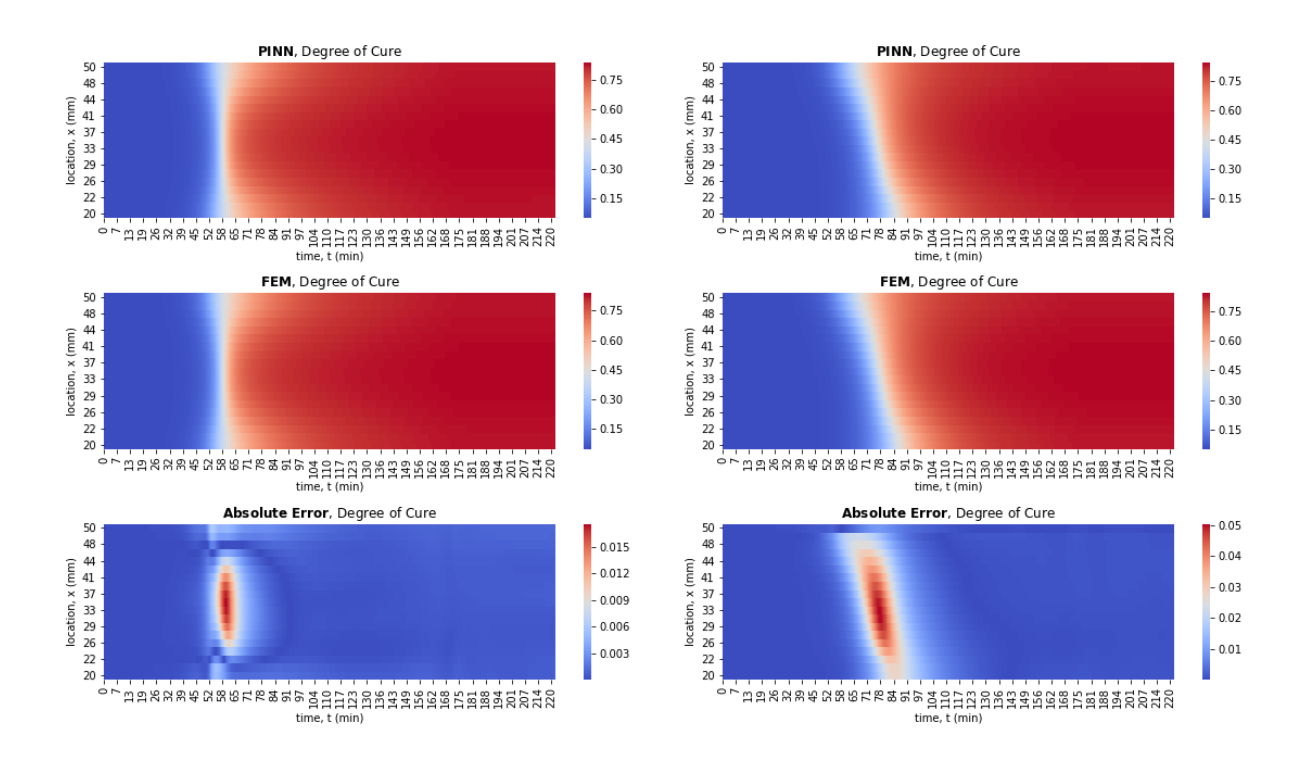


Figure 7: PINN and FEM degree of cure predictions for (Left) case study 1 and (Right) case study 2.

# 4.2. Effect of adaptive loss weights technique

To highlight the importance of employing the adaptive loss weights presented in Section 3.4, the performance of the proposed PINN without such dynamic update of loss weights is presented here. For the case study 1, the evolution of losses associated with initial and boundary conditions for both temperature and degree of cure are shown in Fig. 10 where significantly better convergence is observed when the adaptive loss weight method is used. The error in temperature and degree of cure predictions are also shown in Fig. 11 where significantly higher accuracy in the predictions is observed for the training with adaptive loss weight technique as a consequence of network balanced training. The error of prediction is about 8 and 10 times higher for temperature and degree of cure, respectively, if constant loss weights are used.

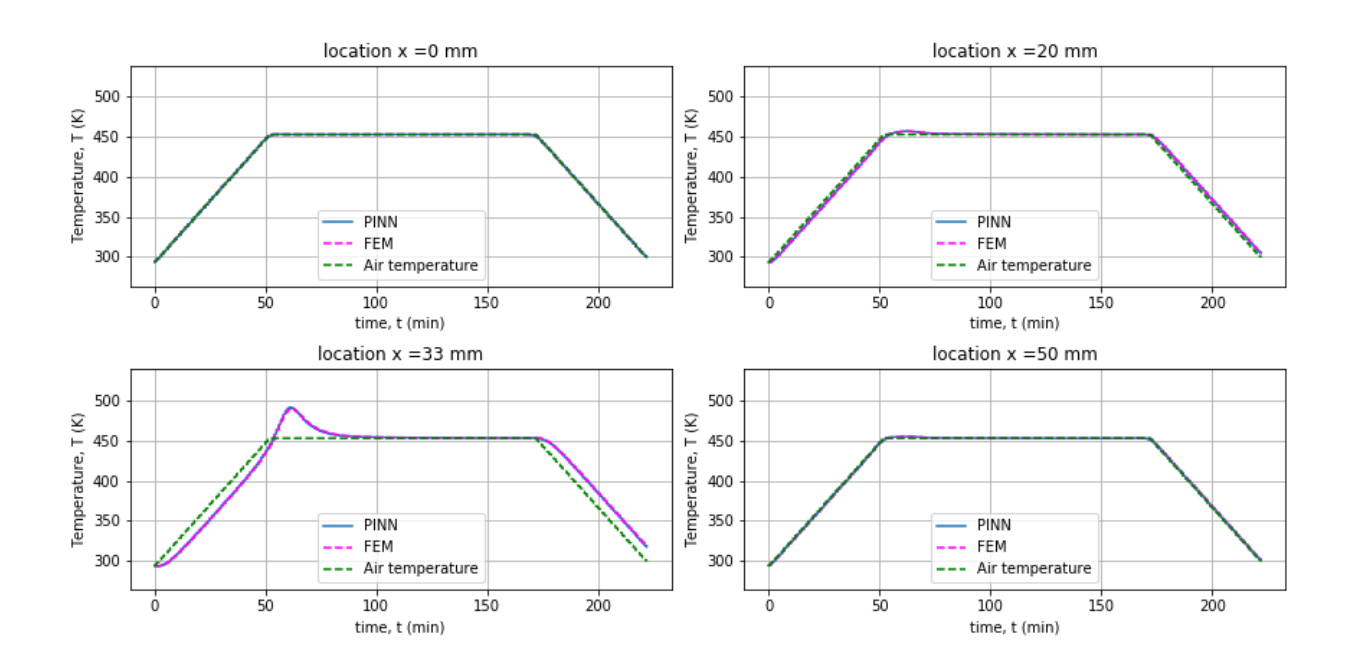


Figure 8: Temperature history for case study 1 (prescribed temperature at boundaries) at tool bottom boundary ( $x=0\,\mathrm{mm}$ ), tool-composite intersection ( $x=20\,\mathrm{mm}$ ), middle of composite ( $x=35\,\mathrm{mm}$ ), and composite boundary top ( $x=50\,\mathrm{mm}$ ).

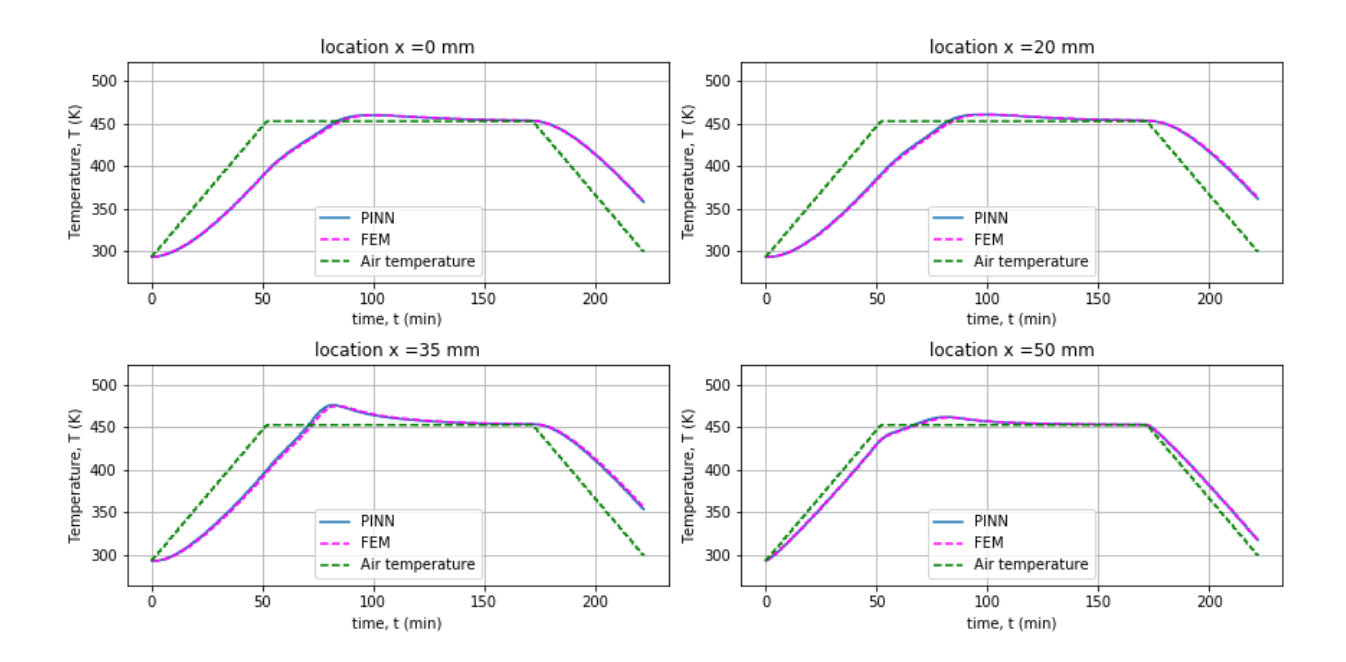


Figure 9: Temperature history for case study 2 (convective temperature at boundaries) at tool bottom boundary ( $x=0\,\mathrm{mm}$ ), tool-composite intersection ( $x=20\,\mathrm{mm}$ ), middle of composite ( $x=35\,\mathrm{mm}$ ), and composite boundary top ( $x=50\,\mathrm{mm}$ ).

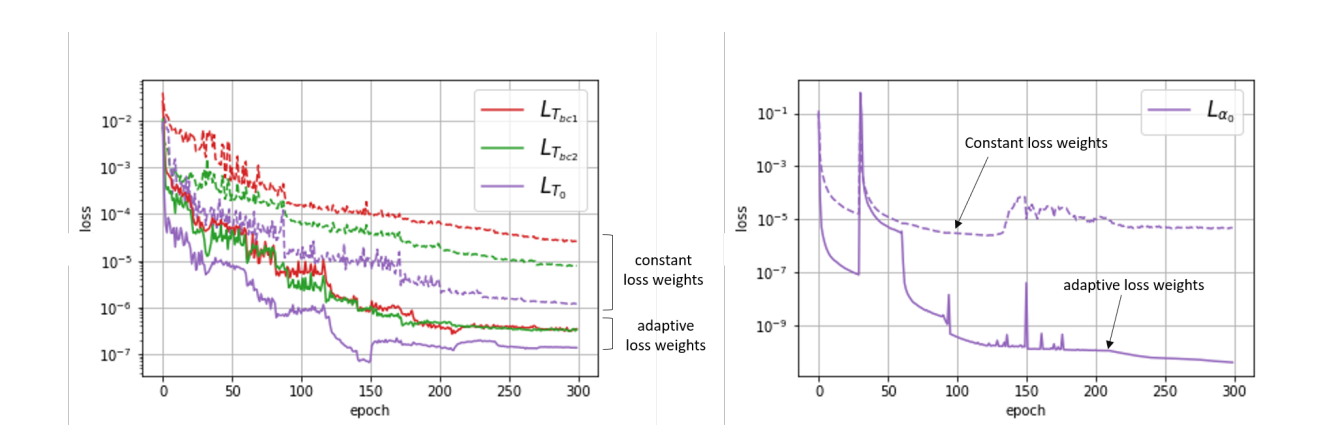


Figure 10: Evolution of initial and boundary conditions loss terms for case study 1 for optimization with constant and adaptive loss weights (Left) temperature (Right) degree of cure.

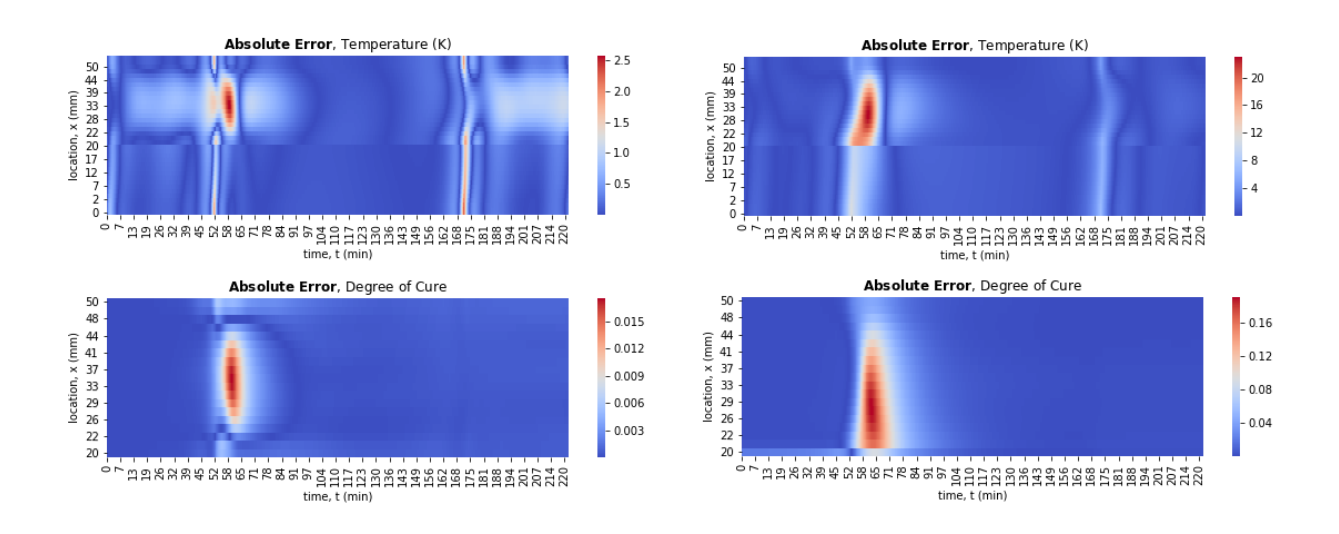


Figure 11: Effect of adaptive loss weight algorithm on error between PINN and FEM predictions for case study 1 (Left) training with adaptive loss technique (Right) training with constant loss weights.

#### 5. Conclusions

In this study, we present a PINN framework for modelling of exothermic heat transfer in a composite-tool system undergoing a full cure-cycle. The proposed PINN is a feed-forward neural network that tackles solution of the two coupled differential equations, namely, the exothermic heat transfer and resin reaction which govern the distribution and evolution of temperature and degree of cure in the composite and tool materials.

A disjointed network architecture is employed to utilize independent networks parameters for the output field variables, i.e. temperature and degree of cure. A sequential approach for training of the proposed disjointed PINN is presented that overcomes instability in the training of the PINN. In the training process, the network parameters are constrained through introduction of physics-based loss functions. Additionally, the standard PINN is modified to capture discontinuities of solution variables and/or their derivatives as a consequence of material discontinuities in the solution domain. The continuity of physical quantities, such as heat flux, are maintained using additional physics-based loss terms. We also employed the adaptive loss weight algorithm based on the scaling gradient of different terms for a robust training of the neural network. Comparisons are made between the numerical results from PINN and those obtained from classical numerical methods which demonstrate the accuracy of the proposed methodology in predicting the temperature and degree of cure.

The proposed PINN does not require labeled data generated in advance using high fidelity simulation tools. It also does not rely on the domain discretization which is typically done in the classical numerical methods. Such characteristics along with the accuracy in predictions of solution variables offers the possibility of using the proposed PINN for surrogate modelling of composite materials processing as well as probabilistic modelling, optimization, uncertainty quantification, and real-time monitoring during processing.

#### Acknowledgments

The authors would like to acknowledge the financial support for this research provided by the Natural Sciences and Engineering Research Council (NSERC) through Alliance grant with Convergent Manufacturing Technologies Inc. (CMT), as the industrial partner.

# Appendix A. An unrealistically thick composite-tool example

The distribution of temperature T and degree of cure  $\alpha$  is affected significantly by the size of composite and tool. To demonstrate the accuracy of the proposed PINN for a wide range of material size, results of the exothermic heat transfer model an on an extreme and unrealistic composite-tool system with  $Lc=300\,\mathrm{mm}$  and  $L_t=200\,\mathrm{mm}$  corresponding to the case studies 3 and 4 in Table 3 are presented here. The temperature and degree of cure are shown in Figs. A.12 and A.13 where again a good match between PINN predictions and those of FEM from RAVEN software is observed. To highlight the accuracy of the PINN, the temperature along the length of the tool and composite is shown in Fig. A.14 where the extreme and high discontinuity of temperature spatial derivative is observed.

Such performance is a direct result of neural network decomposition at the composite-tool intersection point as discussed in Section 3.2 and shown in Fig. 5.

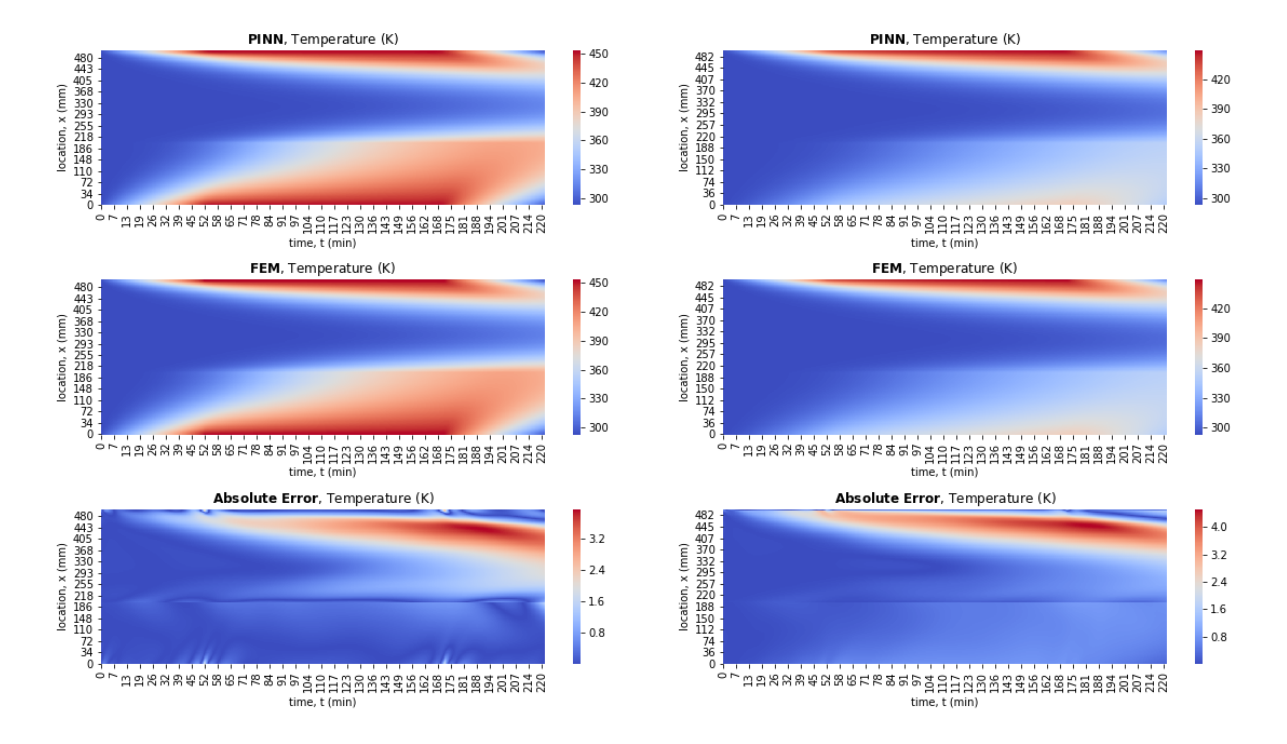


Figure A.12: PINN and FEM degree of cure predictions for (Left) case study 3 and (Right) case study 4.

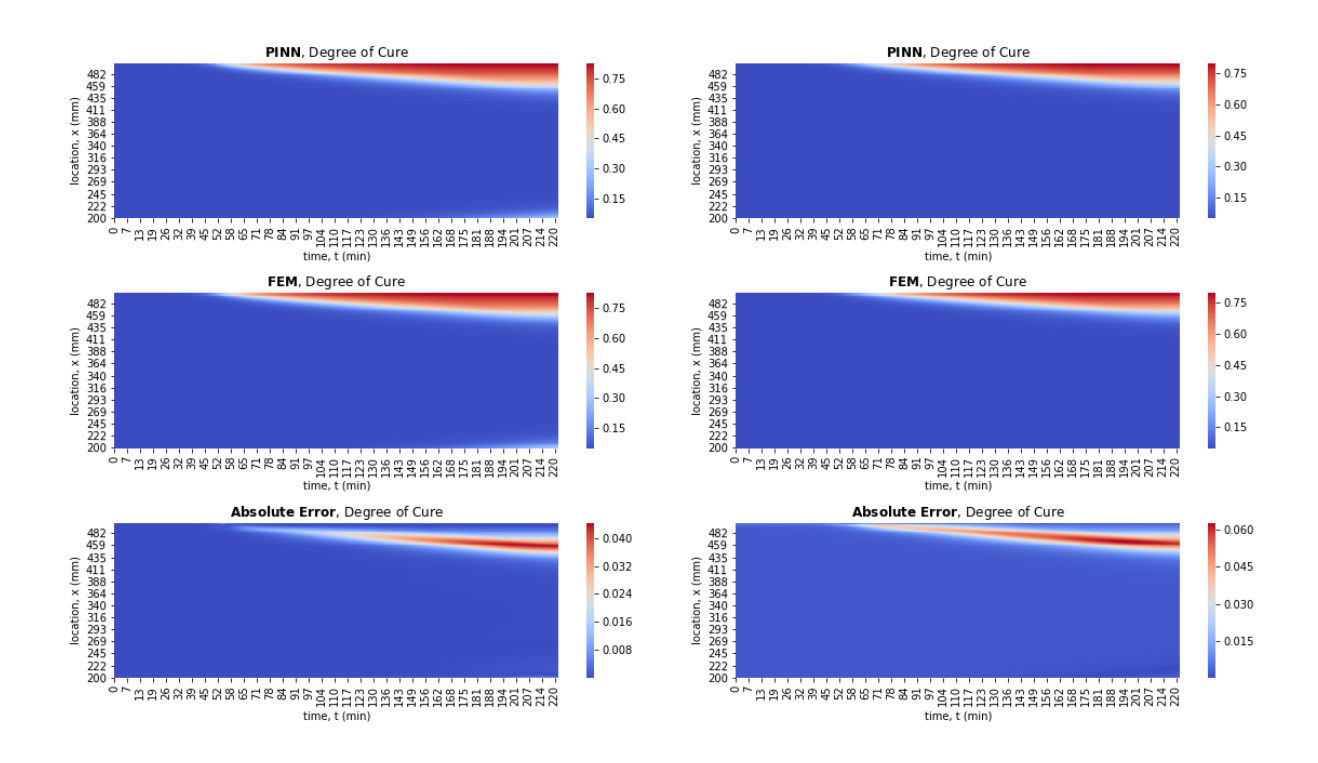


Figure A.13: PINN and FEM degree of cure predictions for (Left) case study 3 and (Right) case study 4.

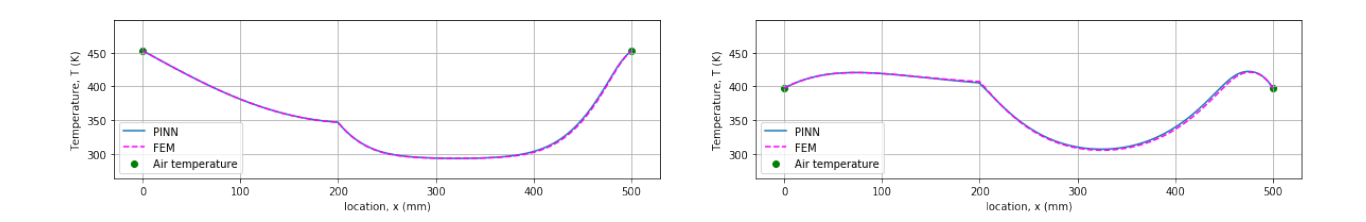


Figure A.14: Temperature distribution for case study 3 (prescribed temperature at boundaries) (Left) at  $t = 90 \,\text{min}$  and (Right) at time  $t = 190 \,\text{min}$ .

#### References

- [1] Flake C Campbell Jr. Manufacturing processes for advanced composites. elsevier, 2003.
- [2] Andrew Johnston, Pascal Hubert, Göran Fernlund, Reza Vaziri, and Anoush Poursartip. Process modeling of composite structures employing a virtual autoclave concept. *Science and Engineering of Composite Materials*, 5:235–252, 1996.
- [3] Nicolas Boyard. Heat Transfer in Polymer Composite Materials: Forming Processes. John Wiley & Sons, 2016.
- [4] Olek C Zienkiewicz, Robert L Taylor, and Jian Z Zhu. The finite element method: its basis and fundamentals. Elsevier, 2005.
- [5] Philippe Boisse, Bassem Zouari, and Alain Gasser. A mesoscopic approach for the simulation of woven fibre composite forming. *Composites science and technology*, 65(3-4):429–436, 2005.
- [6] Nahiene Hamila, Philippe Boisse, Francis Sabourin, and Michel Brunet. A semi-discrete shell finite element for textile composite reinforcement forming simulation. *International journal for numerical methods in engineering*, 79(12):1443–1466, 2009.
- [7] Travis A Bogetti and John W Gillespie Jr. Process-induced stress and deformation in thick-section thermoset composite laminates. *Journal of composite materials*, 26(5):626–660, 1992.
- [8] Travis A Bogetti and John W Gillespie Jr. Two-dimensional cure simulation of thick thermosetting composites. *Journal of composite materials*, 25(3):239–273, 1991.
- [9] Hua Tan and Krishna M Pillai. Multiscale modeling of unsaturated flow in dual-scale fiber preforms of liquid composite molding i: Isothermal flows. Composites Part A: Applied Science and Manufacturing, 43(1):1–13, 2012.
- [10] Ram V Mohan, ND Ngo, and Kumar K Tamma. On a pure finite-element-based methodology for resin transfer molds filling simulations. *Polymer Engineering & Science*, 39(1):26–43, 1999.
- [11] MV Bruschke and Suresh G Advani. A finite element/control volume approach to mold filling in anisotropic porous media. *Polymer composites*, 11(6):398–405, 1990.
- [12] Sina Amini Niaki, Alireza Forghani, Reza Vaziri, and Anoush Poursartip. A two-phase integrated flow-stress process model for composites with application to highly compressible phases. *Mechanics of Materials*, 109:51–66, 2017.
- [13] Sina Amini Niaki, Alireza Forghani, Reza Vaziri, and Anoush Poursartip. A three-phase integrated flow-stress model for processing of composites. *Mechanics of Materials*, 117:152–164, 2018.
- [14] Sina Amini Niaki, Alireza Forghani, Reza Vaziri, and Anoush Poursartip. An orthotropic integrated flow-stress model for process simulation of composite materials—part ii: Three-phase systems. *Journal of Manufacturing Science and Engineering*, 141(3), 01 2019. ISSN 1087-1357. 031010.
- [15] Sina Amini Niaki, Alireza Forghani, Reza Vaziri, and Anoush Poursartip. An orthotropic integrated flow-stress model for process simulation of composite materials—part ii: Three-phase systems. *Journal of Manufacturing Science and Engineering*, 141(3), 01 2019. ISSN 1087-1357. 031011.
- [16] Yann LeCun, Yoshua Bengio, and Geoffrey Hinton. Deep learning. nature, 521(7553):436–444, 2015.
- [17] James Bergstra, Olivier Breuleux, Frédéric Bastien, Pascal Lamblin, Razvan Pascanu, Guillaume Desjardins, Joseph Turian, David Warde-Farley, and Yoshua Bengio. Theano: a cpu and gpu math expression compiler. In *Proceedings of the Python for scientific computing conference (SciPy)*, pages 1–7. Austin, TX, 2010.
- [18] Atılım Günes Baydin, Barak A Pearlmutter, Alexey Andreyevich Radul, and Jeffrey Mark Siskind. Automatic differentiation in machine learning: a survey. *The Journal of Machine Learning Research*, 18(1):5595–5637, 2017.
- [19] Yu M Ermoliev and RJ-B Wets. Numerical techniques for stochastic optimization. Springer-Verlag, 1988.
- [20] Anuj Karpatne, Gowtham Atluri, James H Faghmous, Michael Steinbach, Arindam Banerjee, Auroop Ganguly, Shashi Shekhar, Nagiza Samatova, and Vipin Kumar. Theory-guided data science: A new paradigm for scientific discovery from data. *IEEE Transactions on knowledge and data engineering*, 29 (10):2318–2331, 2017.

- [21] Nicholas Wagner and James M Rondinelli. Theory-guided machine learning in materials science. Frontiers in Materials, 3:28, 2016.
- [22] Phoebe MR DeVries, Fernanda Viégas, Martin Wattenberg, and Brendan J Meade. Deep learning of aftershock patterns following large earthquakes. *Nature*, 560(7720):632–634, 2018.
- [23] Liang Liang, Minliang Liu, Caitlin Martin, and Wei Sun. A deep learning approach to estimate stress distribution: a fast and accurate surrogate of finite-element analysis. *Journal of The Royal Society Interface*, 15(138):20170844, 2018.
- [24] Maziar Raissi, Paris Perdikaris, and George E Karniadakis. Physics-informed neural networks: A deep learning framework for solving forward and inverse problems involving nonlinear partial differential equations. *Journal of Computational Physics*, 378:686–707, 2019.
- [25] Andrew J Meade Jr and Alvaro A Fernandez. The numerical solution of linear ordinary differential equations by feedforward neural networks. *Mathematical and Computer Modelling*, 19(12):1–25, 1994.
- [26] Dimitris C Psichogios and Lyle H Ungar. A hybrid neural network-first principles approach to process modeling. *AIChE Journal*, 38(10):1499–1511, 1992.
- [27] Isaac E Lagaris, Aristidis Likas, and Dimitrios I Fotiadis. Artificial neural networks for solving ordinary and partial differential equations. *IEEE transactions on neural networks*, 9(5):987–1000, 1998.
- [28] Guofei Pang and George Em Karniadakis. Physics-informed learning machines for partial differential equations: Gaussian processes versus neural networks. In *Emerging Frontiers in Nonlinear Science*, pages 323–343. Springer, 2020.
- [29] Justin Sirignano and Konstantinos Spiliopoulos. Dgm: A deep learning algorithm for solving partial differential equations. *Journal of computational physics*, 375:1339–1364, 2018.
- [30] Jens Berg and Kaj Nyström. A unified deep artificial neural network approach to partial differential equations in complex geometries. *Neurocomputing*, 317:28–41, 2018.
- [31] Cosmin Anitescu, Elena Atroshchenko, Naif Alajlan, and Timon Rabczuk. Artificial neural network methods for the solution of second order boundary value problems. *Computers, Materials and Continua*, 59(1):345–359, 2019.
- [32] Ehsan Kharazmi, Zhongqiang Zhang, and George Em Karniadakis. Variational physics-informed neural networks for solving partial differential equations. arXiv preprint arXiv:1912.00873, 2019.
- [33] Luning Sun, Han Gao, Shaowu Pan, and Jian-Xun Wang. Surrogate modeling for fluid flows based on physics-constrained deep learning without simulation data. Computer Methods in Applied Mechanics and Engineering, 361:112732, 2020.
- [34] Ameya D Jagtap, Ehsan Kharazmi, and George Em Karniadakis. Conservative physics-informed neural networks on discrete domains for conservation laws: Applications to forward and inverse problems. Computer Methods in Applied Mechanics and Engineering, 365:113028, 2020.
- [35] Vien Minh Nguyen-Thanh, Xiaoying Zhuang, and Timon Rabczuk. A deep energy method for finite deformation hyperelasticity. European Journal of Mechanics-A/Solids, 80:103874, 2020.
- [36] Somdatta Goswami, Cosmin Anitescu, Souvik Chakraborty, and Timon Rabczuk. Transfer learning enhanced physics informed neural network for phase-field modeling of fracture. *Theoretical and Applied Fracture Mechanics*, 106:102447, 2020.
- [37] Ehsan Haghighat, Maziar Raissi, Adrian Moure, Hector Gomez, and Ruben Juanes. A deep learning framework for solution and discovery in solid mechanics. arXiv preprint arXiv:2003.02751, 2020.
- [38] QiZhi He, David Barajas-Solano, Guzel Tartakovsky, and Alexandre M Tartakovsky. Physics-informed neural networks for multiphysics data assimilation with application to subsurface transport. *Advances in Water Resources*, page 103610, 2020.
- [39] Ehsan Kharazmi, Zhongqiang Zhang, and George Em Karniadakis. hp-vpinns: Variational physics-informed neural networks with domain decomposition. arXiv preprint arXiv:2003.05385, 2020.
- [40] Andrew A Johnston. An integrated model of the development of process-induced deformation in autoclave processing of composite structures. PhD thesis, University of British Columbia, 1997.
- [41] Navid Zobeiry and Keith D Humfeld. A physics-informed machine learning approach for solving heat transfer equation in advanced manufacturing and engineering applications. arXiv preprint arXiv:2010.02011, 2020.

- [42] P Sibi, S Allwyn Jones, and P Siddarth. Analysis of different activation functions using back propagation neural networks. *Journal of theoretical and applied information technology*, 47(3):1264–1268, 2013.
- [43] Dongkun Zhang, Lu Lu, Ling Guo, and George Em Karniadakis. Quantifying total uncertainty in physics-informed neural networks for solving forward and inverse stochastic problems. *Journal of Computational Physics*, 397:108850, 2019.
- [44] Francisco Sahli Costabal, Yibo Yang, Paris Perdikaris, Daniel E Hurtado, and Ellen Kuhl. Physics-informed neural networks for cardiac activation mapping. Frontiers in Physics, 8:42, 2020.
- [45] R Timothy Marler and Jasbir S Arora. The weighted sum method for multi-objective optimization: new insights. Structural and multidisciplinary optimization, 41(6):853–862, 2010.
- [46] Sifan Wang, Yujun Teng, and Paris Perdikaris. Understanding and mitigating gradient pathologies in physics-informed neural networks. arXiv preprint arXiv:2001.04536, 2020.
- [47] TE Twardowski, SE Lin, and PH Geil. Curing in thick composite laminates: experiment and simulation. Journal of composite materials, 27(3):216–250, 1993.
- [48] Martín Abadi, Paul Barham, Jianmin Chen, Zhifeng Chen, Andy Davis, Jeffrey Dean, Matthieu Devin, Sanjay Ghemawat, Geoffrey Irving, Michael Isard, et al. Tensorflow: A system for large-scale machine learning. In 12th {USENIX} symposium on operating systems design and implementation ({OSDI} 16), pages 265–283, 2016.
- [49] Adam Paszke, Sam Gross, Francisco Massa, Adam Lerer, James Bradbury, Gregory Chanan, Trevor Killeen, Zeming Lin, Natalia Gimelshein, Luca Antiga, et al. Pytorch: An imperative style, high-performance deep learning library. In Advances in neural information processing systems, pages 8026–8037, 2019.
- [50] François Chollet et al. Keras. https://github.com/fchollet/keras, 2015.
- [51] Lu Lu, Xuhui Meng, Zhiping Mao, and George E Karniadakis. Deepxde: A deep learning library for solving differential equations. arXiv preprint arXiv:1907.04502, 2019.
- [52] Ehsan Haghighat and Ruben Juanes. Sciann: A keras/tensorflow wrapper for scientific computations and physics-informed deep learning using artificial neural networks. *Computer Methods in Applied Mechanics and Engineering*, 373:113552, 2021. ISSN 0045-7825. doi: https://doi.org/10.1016/j.cma. 2020.113552. URL http://www.sciencedirect.com/science/article/pii/S0045782520307374.
- [53] Diederik P Kingma and Jimmy Ba. Adam: A method for stochastic optimization. *Proceedings of the* 3rd International Conference on Learning Representations (ICLR), pages 1–15, 2015.
- [54] Convergent Manufacturing Technologies. Inc. RAVEN 3.13.1. www.convergent.ca/products/raven-simulation-software, 2020.